

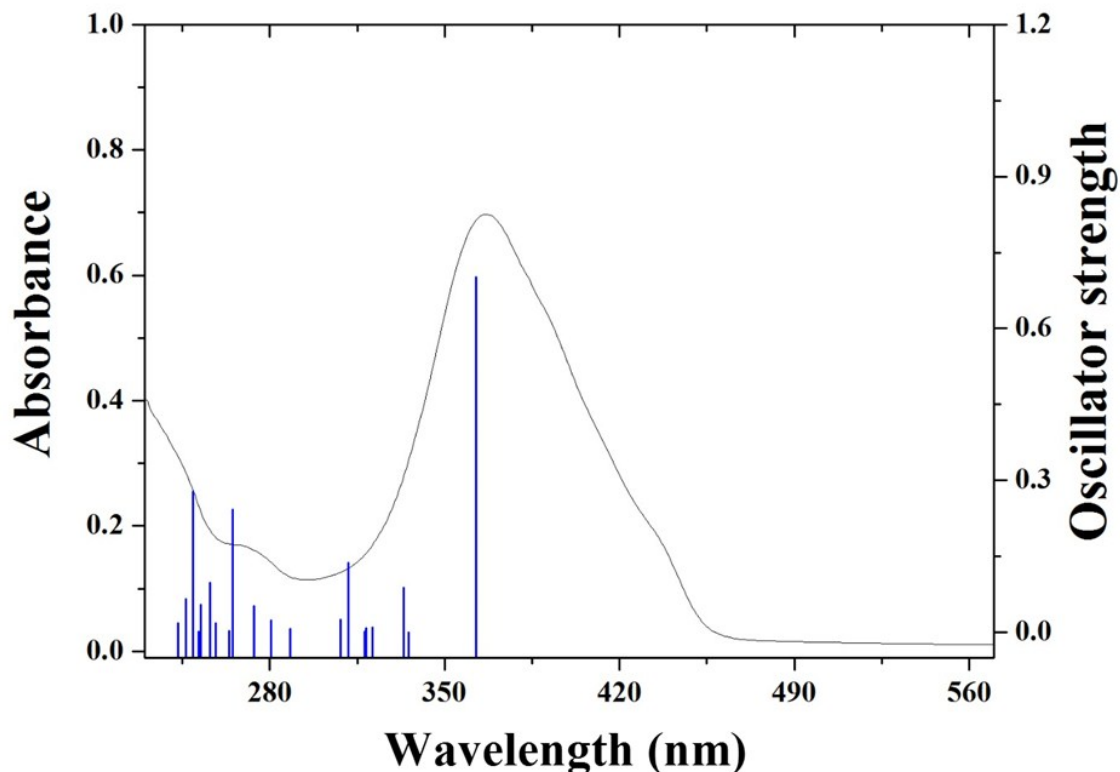
## Supporting Information

### **Distinction between Mn(III) and Mn(II) by using a colorimetric chemosensor in aqueous solution**

Seul Ah Lee, Jae Jun Lee, Ga Rim You, Ye Won Choi, Cheal Kim\*

*Department of Fine Chemistry and Department of Interdisciplinary Bio IT Materials, Seoul National University of Science and Technology, Seoul 139-743, Korea. Fax: +82-2-973-9149; Tel: +82-2-970-6693; E-mail: [chealkim@seoultech.ac.kr](mailto:chealkim@seoultech.ac.kr)*

(a)

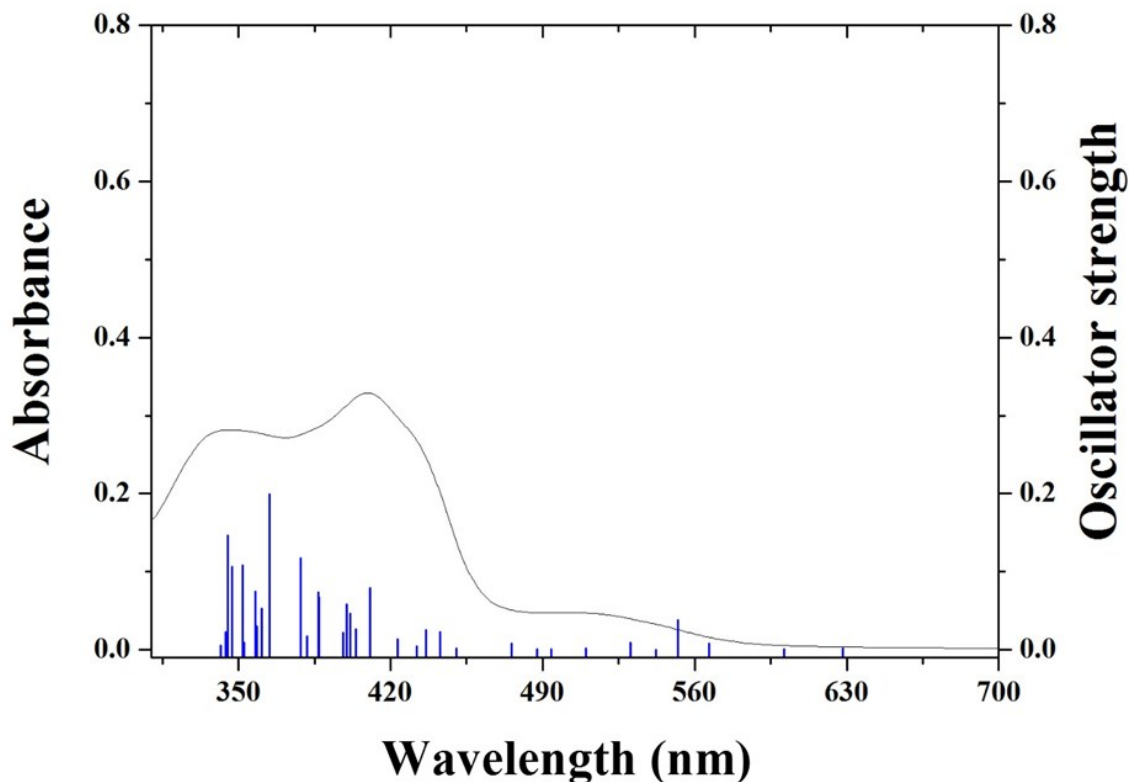


(b)

Excited State 1	Wavelength	Percent (%)	Oscillator strength
H → L	362.50 nm	97 %	0.7023
Excited State 2	Wavelength	Percent (%)	Oscillator strength
H-1 → L+1	335.52 nm	94 %	0.0004
H-1 → L		4 %	

**Table S1.** (a) The theoretical excitation energies and the experimental UV-vis spectrum of **1**. (b) The major electronic transition energies and molecular orbital contributions for **1** (H = HOMO and L = LUMO).

(a)



(b)

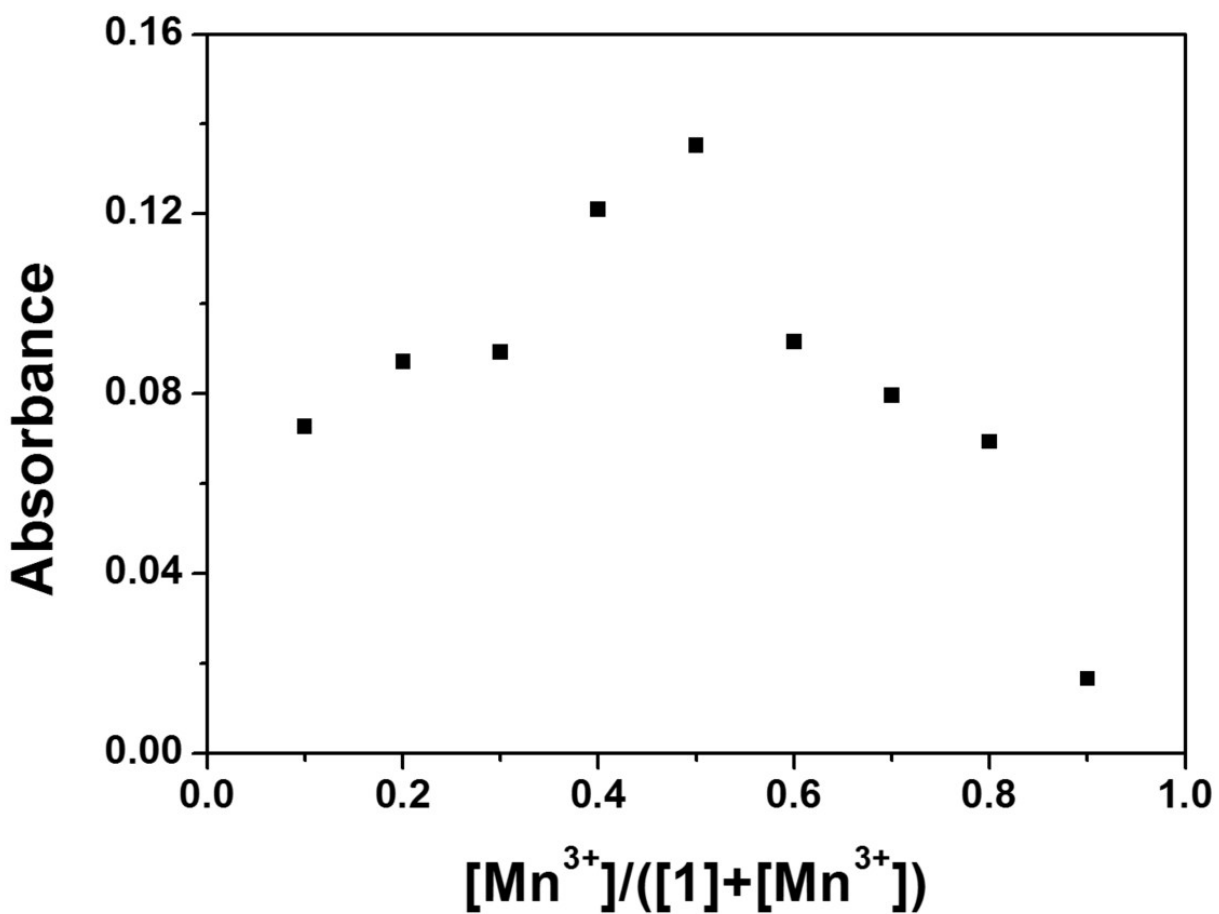
Excited State 10	Wavelength	Percent (%)	Main character	Oscillator strength
H-1 → L ( $\alpha$ )	552.33 nm	5 %	LMCT	0.0386
H-2 → L ( $\alpha$ )		5 %	LMCT	
H-1 → L+1 ( $\alpha$ )		3 %	ICT	
H-6 → L ( $\alpha$ )		2 %	LMCT	
H → L ( $\beta$ )		58 %	LMCT	
H-2 → L ( $\beta$ )		18 %	LMCT	

Excited State 22	Wavelength	Percent (%)	Main character	Oscillator strength
H-2 → L ( $\alpha$ )	410.69 nm	5 %	LMCT	0.0791
H-11 → L ( $\alpha$ )		3 %	d-d transition	
H-2 → L+1 ( $\alpha$ )		2 %	ICT	
H → L+2 ( $\alpha$ )		2 %	ICT	
H → L+2 ( $\beta$ )		22 %	ICT	
H-2 → L ( $\beta$ )		11 %	LMCT	
H-1 → L+2 ( $\beta$ )		11 %	ICT	
H-4 → L ( $\beta$ )		10 %	LMCT	

H-3 → L+2 ( $\beta$ )	2 %	ICT		
H-2 → L+2 ( $\beta$ )	2 %	MLCT		
H-1 → L+3 ( $\beta$ )	2 %	LMCT		
H-1 → L+4 ( $\beta$ )	2 %	ICT		
H → L+3 ( $\beta$ )	2 %	LMCT		
H → L+4 ( $\beta$ )	2 %	ICT		
Excited State 30	Wavelength	Percent (%)	Main character	Oscillator strength
H-4 → L ( $\alpha$ )	378.60 nm	22 %	LMCT	0.1177
H-2 → L+1 ( $\alpha$ )		10 %	ICT	
H-1 → L+1 ( $\alpha$ )		5 %	ICT	
H → L+3 ( $\beta$ )		29 %	LMCT	
H-1 → L+3 ( $\beta$ )		3 %	LMCT	
H-1 → L+4 ( $\beta$ )		3 %	ICT	
H → L+4 ( $\beta$ )		3 %	ICT	
H-2 → L+4 ( $\beta$ )		2 %	ICT	
H → L+2 ( $\beta$ )		2 %	ICT	

**Table S2.** (a) The theoretical excitation energies and the experimental UV-vis spectrum of **1**-Mn<sup>3+</sup>. (b) The major electronic transition energies and molecular orbital contributions for **1**-Mn<sup>3+</sup> (H = HOMO and L = LUMO).



**Fig. S1** Job plot for the binding of **1** with  $\text{Mn}^{3+}$ . Absorbance at 437 nm was plotted as a function of the molar ratio  $[\text{Mn}^{3+}] / ([\mathbf{1}] + [\text{Mn}^{3+}])$ . The total concentrations of  $\text{Mn}^{3+}$  ions with receptor **1** were  $1.0 \times 10^{-5}$  M.

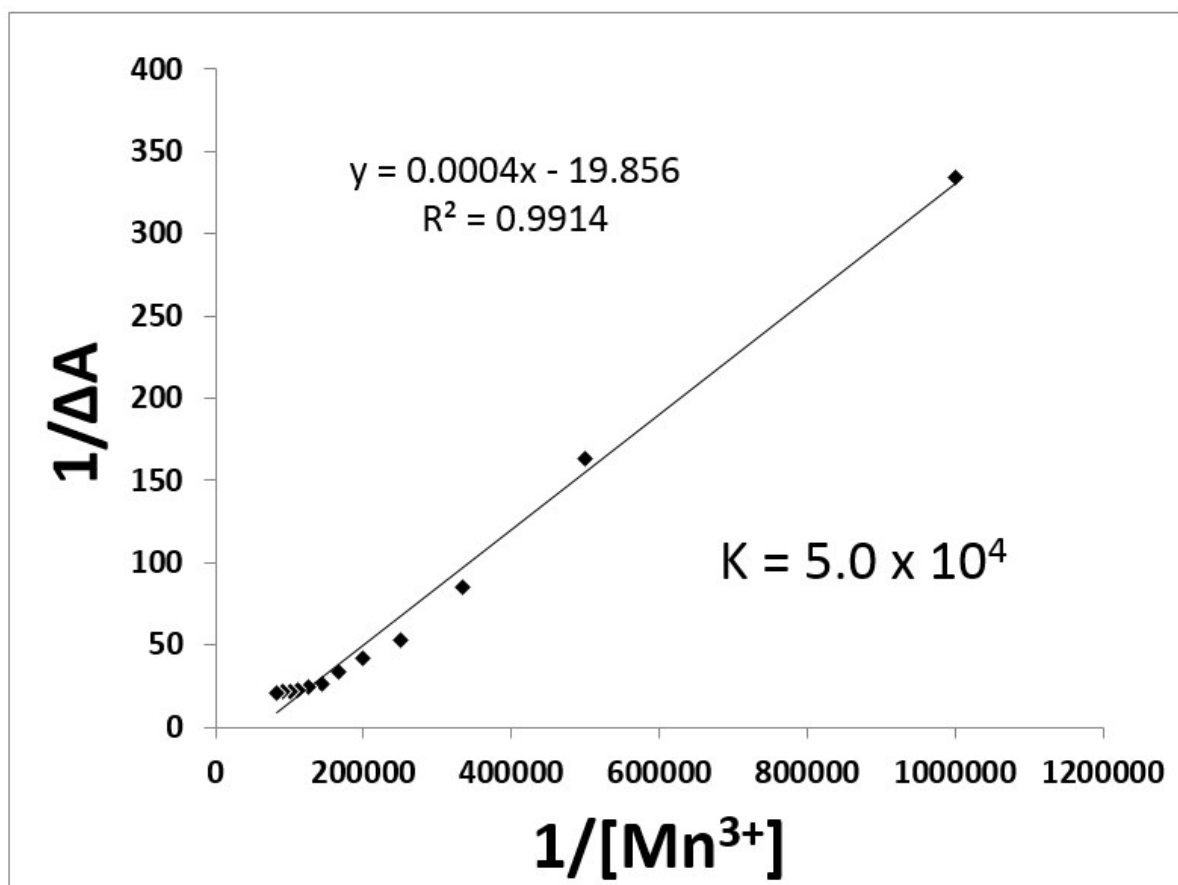


**Fig. S2** Benesi-Hildebrand plot (absorbance at 500 nm) of **1**, assuming a 1:1 stoichiometry for association between **1** and  $\text{Mn}^{3+}$ .

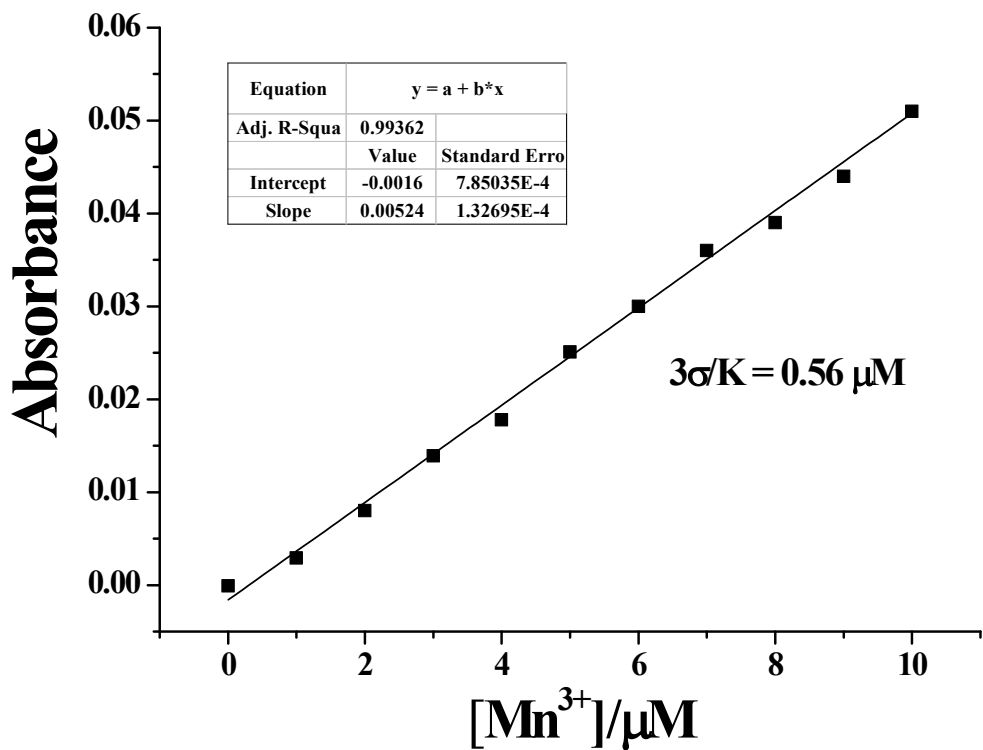
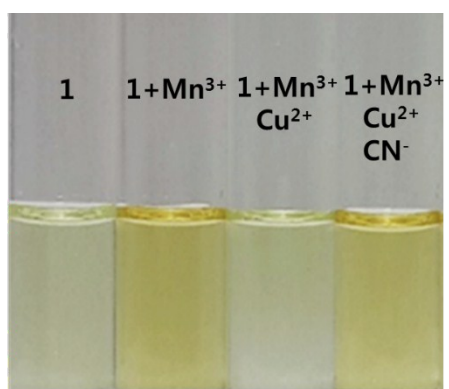


**Fig. S3** Determination of the detection limit based on change in the ratio (absorbance at 500 nm) of **1** (10 μM) with Mn<sup>3+</sup>.

(a)



(b)

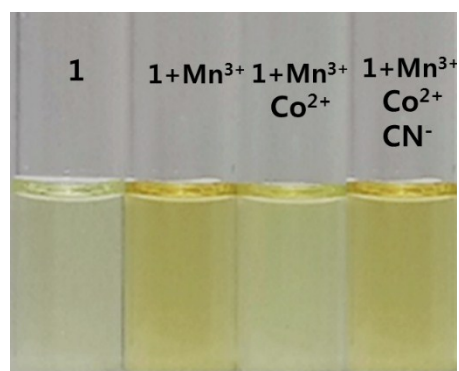


**Fig. S4** (a) Colorimetric changes of **1**-Mn<sup>3+</sup> and **1**-Mn<sup>3+</sup>-Cu<sup>2+</sup> (10  $\mu$ M) in absence or presence of CN<sup>-</sup> (150 equiv). (b) Colorimetric changes of **1**-Mn<sup>3+</sup> and **1**-Mn<sup>3+</sup>-Co<sup>2+</sup> (10  $\mu$ M) in absence or presence of CN<sup>-</sup> (150 equiv).

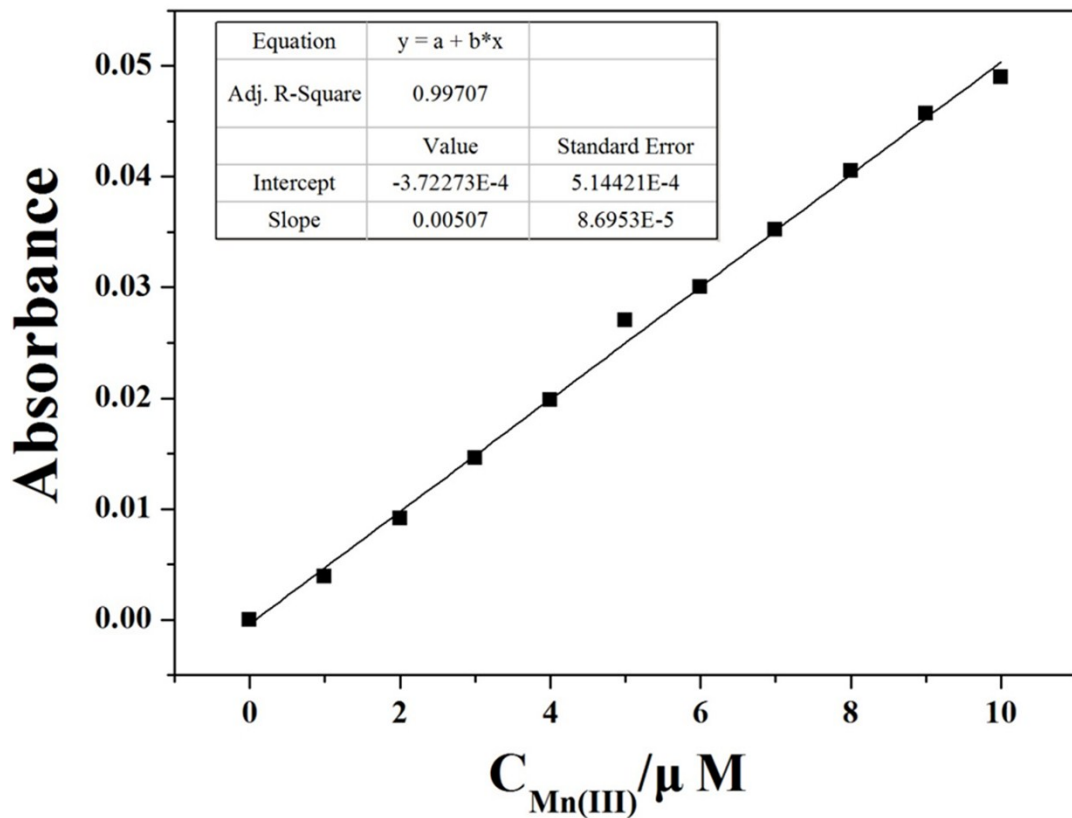


**Fig. S5** UV-vis absorbance (at 500 nm) of **1** as a function of Mn (III) concentration ( $[1] = 30 \mu\text{mol/L}$  and  $[\text{Mn(III)}] = 0.00-10.00 \mu\text{mol/L}$ ). Conditions: all samples were conducted in buffer-CH<sub>3</sub>CN solution (7:3, v/v, 10 mM bis-tris, pH 7.0).

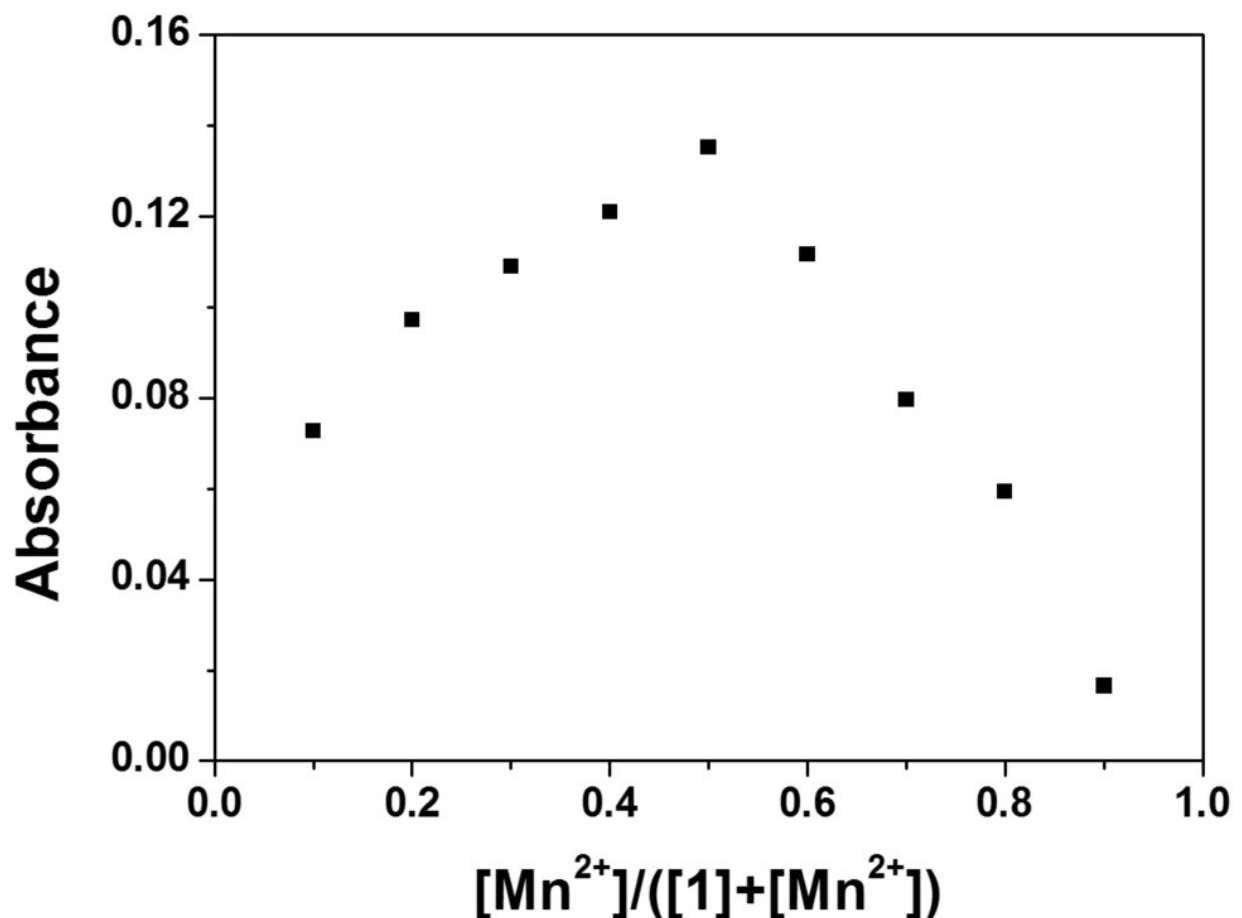


**Fig. S6** Job plot for the binding of **1** with  $Mn^{2+}$ . Absorbance at 437 nm was plotted as a function of the molar ratio  $[Mn^{2+}] / ([1] + [Mn^{2+}])$ . The total concentrations of  $Mn^{2+}$  ions with receptor **1** were  $1.0 \times 10^{-5}$  M.

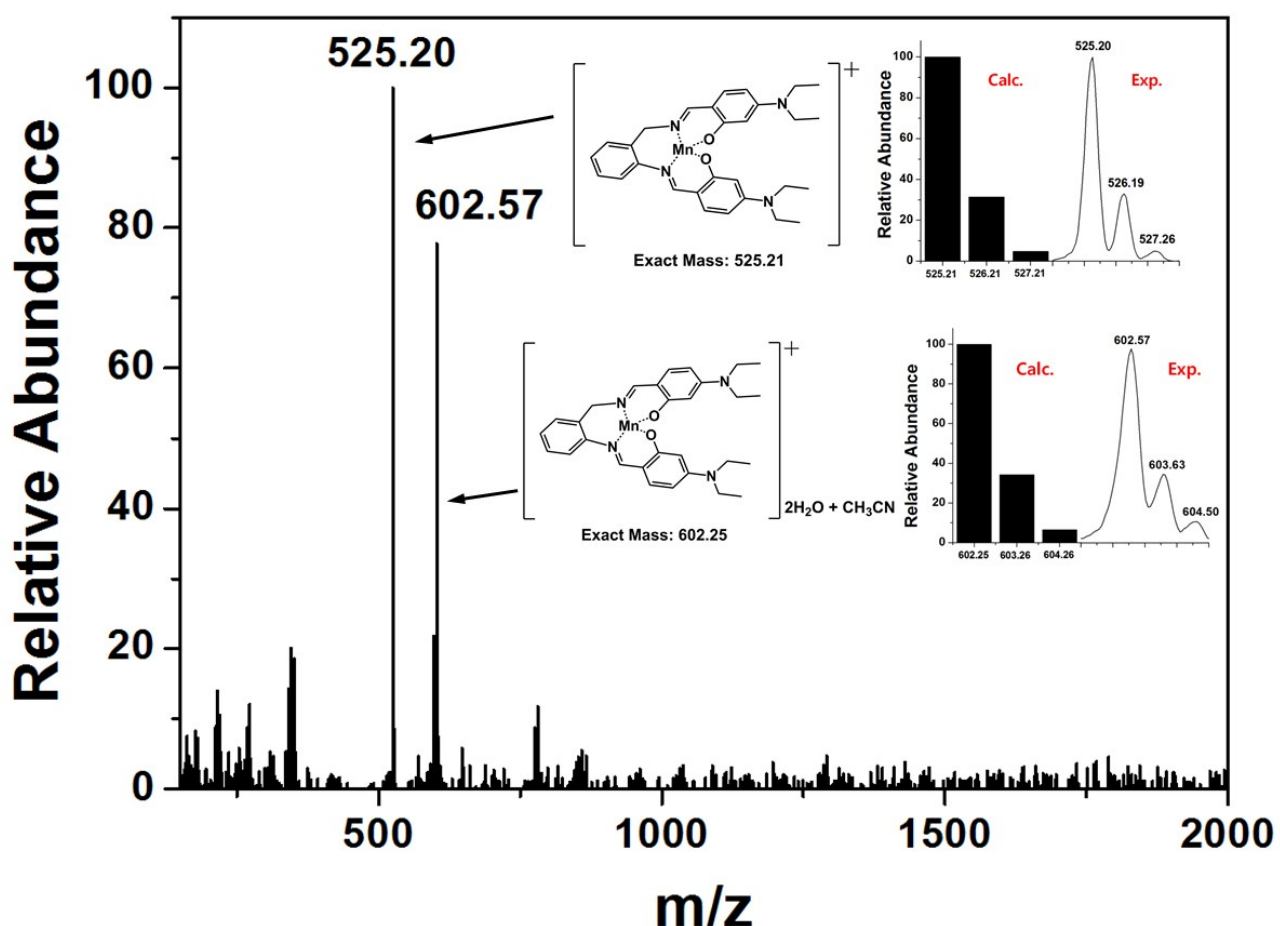


**Fig. S7** Positive-ion electrospray ionization mass spectrum of **1** (100  $\mu\text{M}$ ) upon addition of 1 equiv of  $\text{Mn}^{2+}$ .

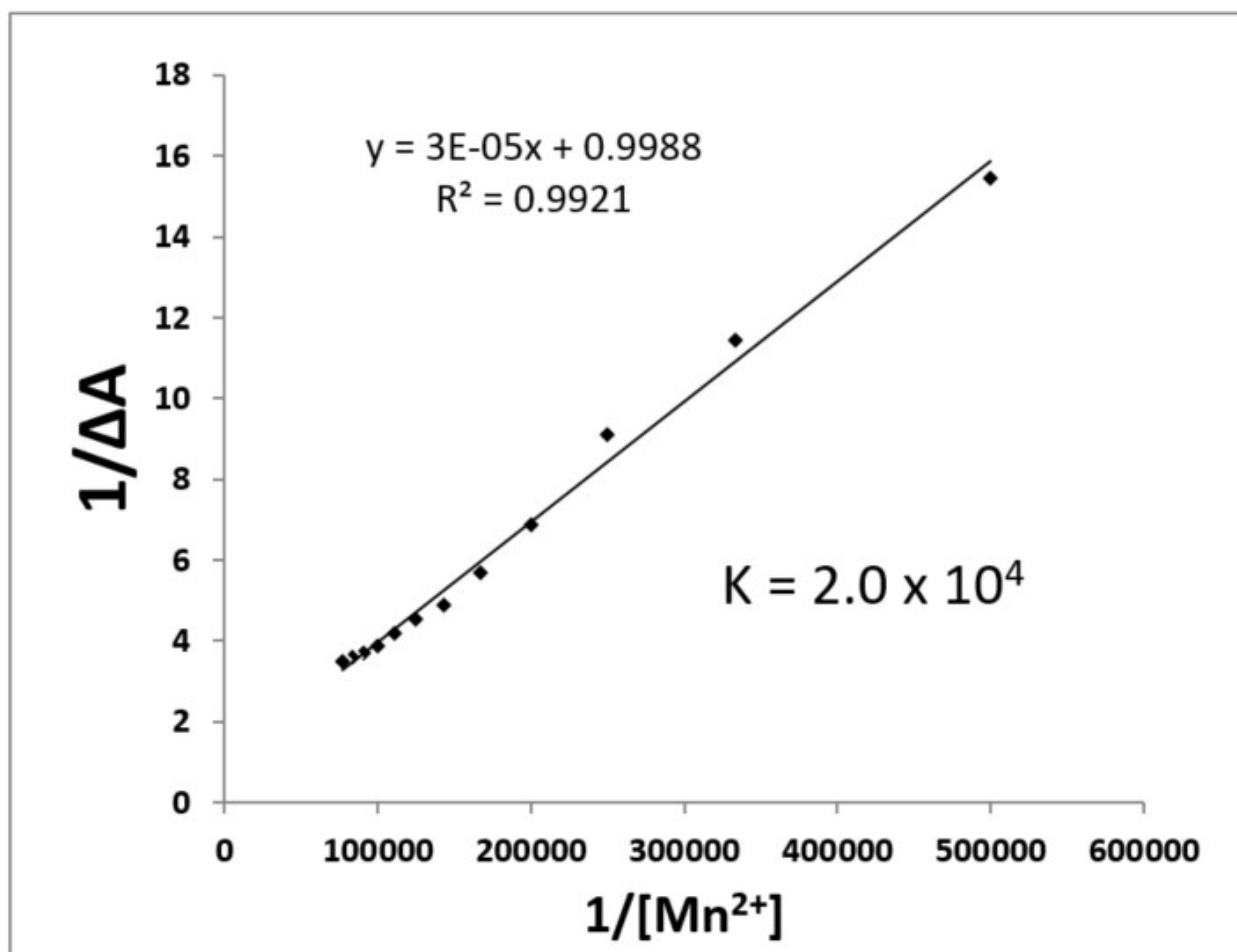


**Fig. S8** Benesi-Hildebrand plot (absorbance at 375 nm) of **1**, assuming a 1:1 stoichiometry for association between **1** and  $\text{Mn}^{2+}$ .

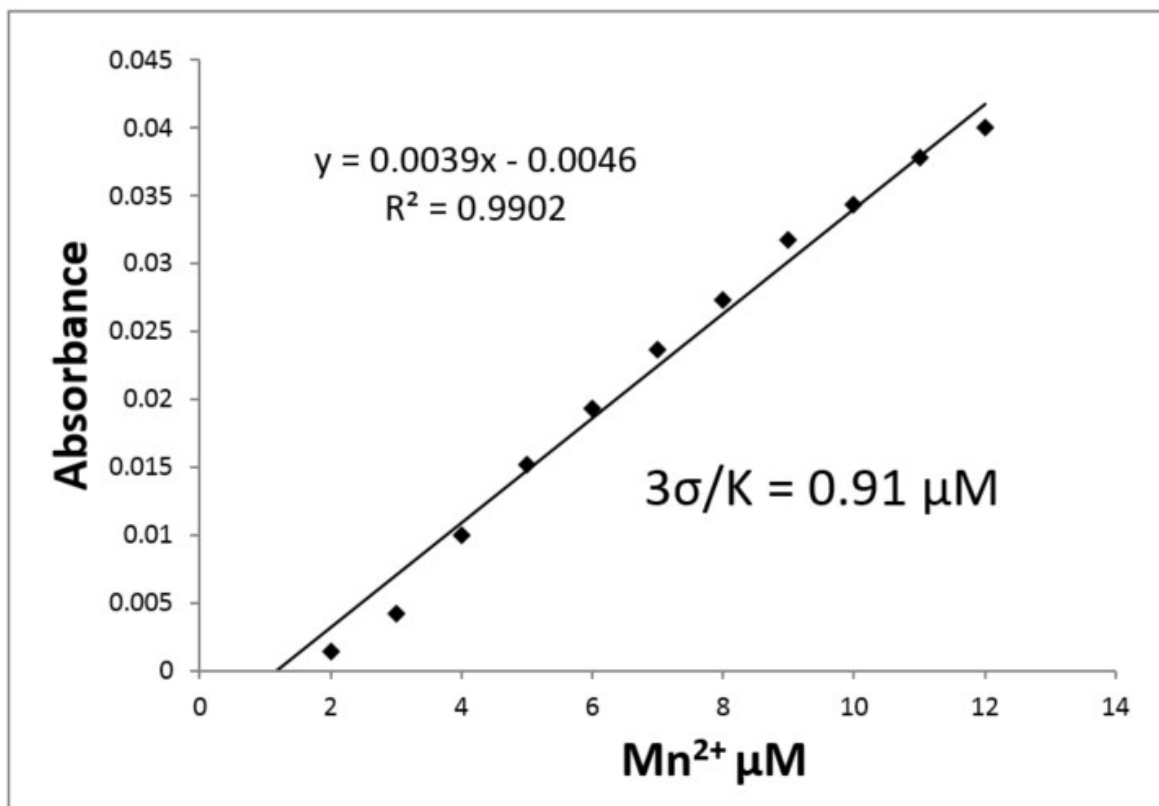
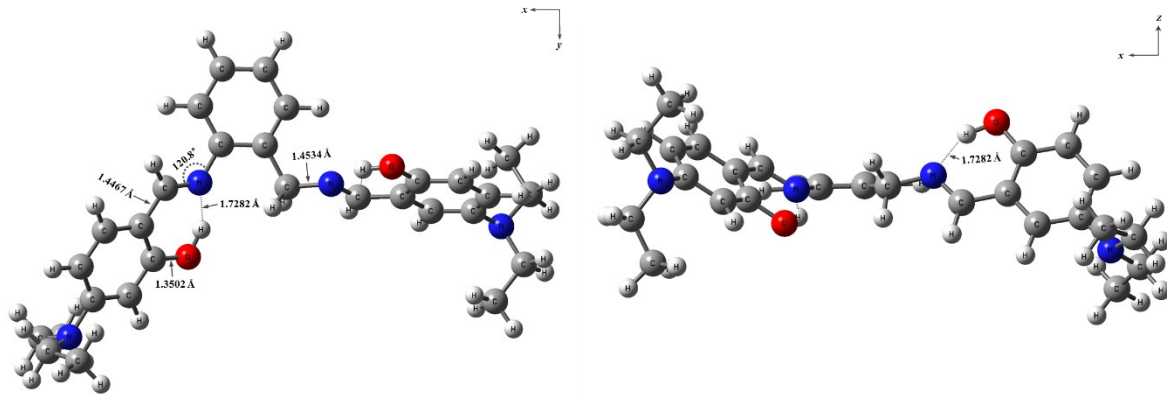


**Fig. S9** Determination of the detection limit based on change in the ratio (absorbance at 500 nm) of **1** (10  $\mu\text{M}$ ) with  $\text{Mn}^{2+}$ .

(a)



(b)

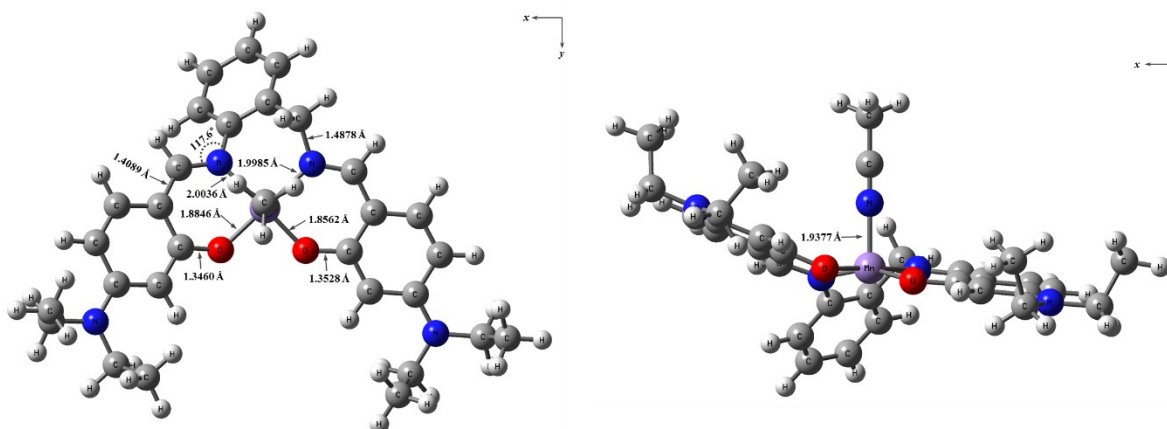


**Fig. S10** The energy-minimized structures of (a) **1** and (b) **1-Mn<sup>3+</sup>** complex.

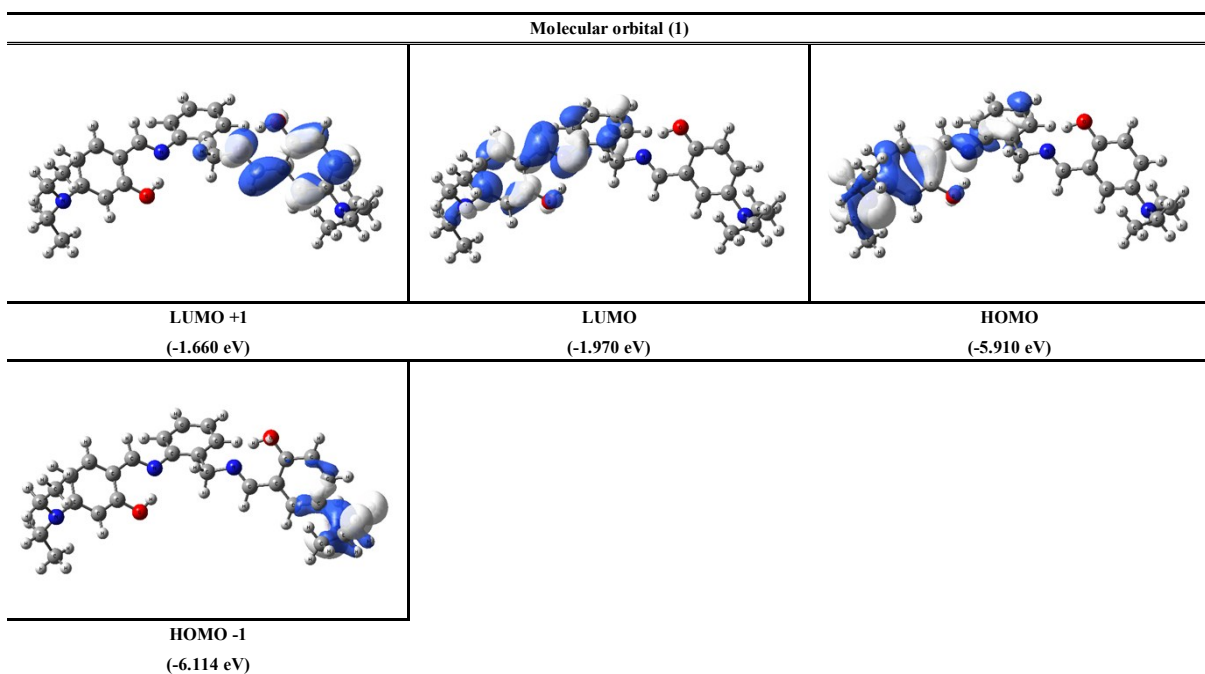


**Fig. S11** Isosurface (0.030 electron bohr<sup>-3</sup>) of molecular orbitals participating in the major singlet excited states of **1**.

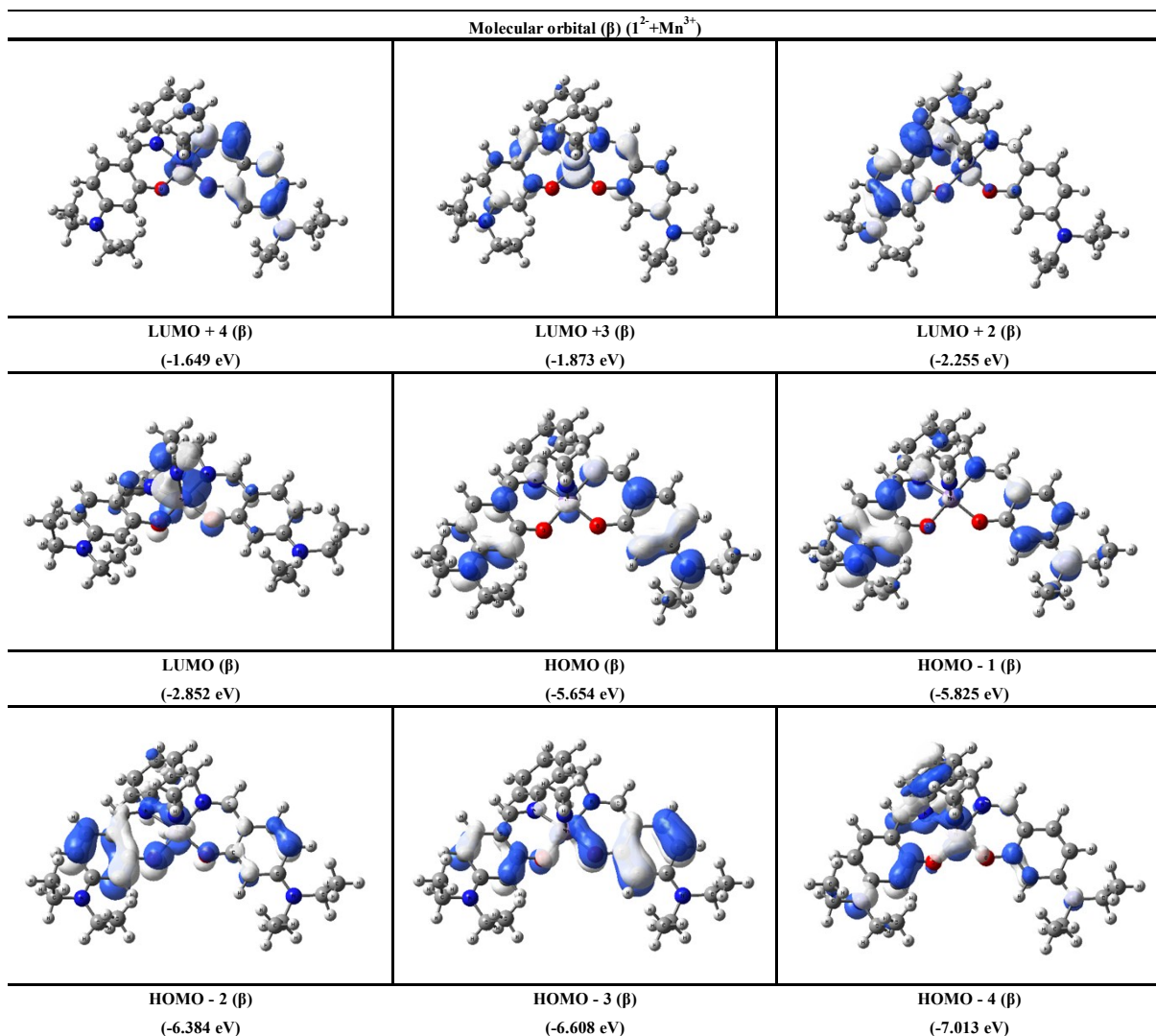


**Fig. S12** Isosurface (0.030 electron bohr<sup>-3</sup>) of molecular orbitals ( $\alpha$  spin) participating in the major singlet excited states of  $\mathbf{1}\text{-Mn}^{3+}$  complex.

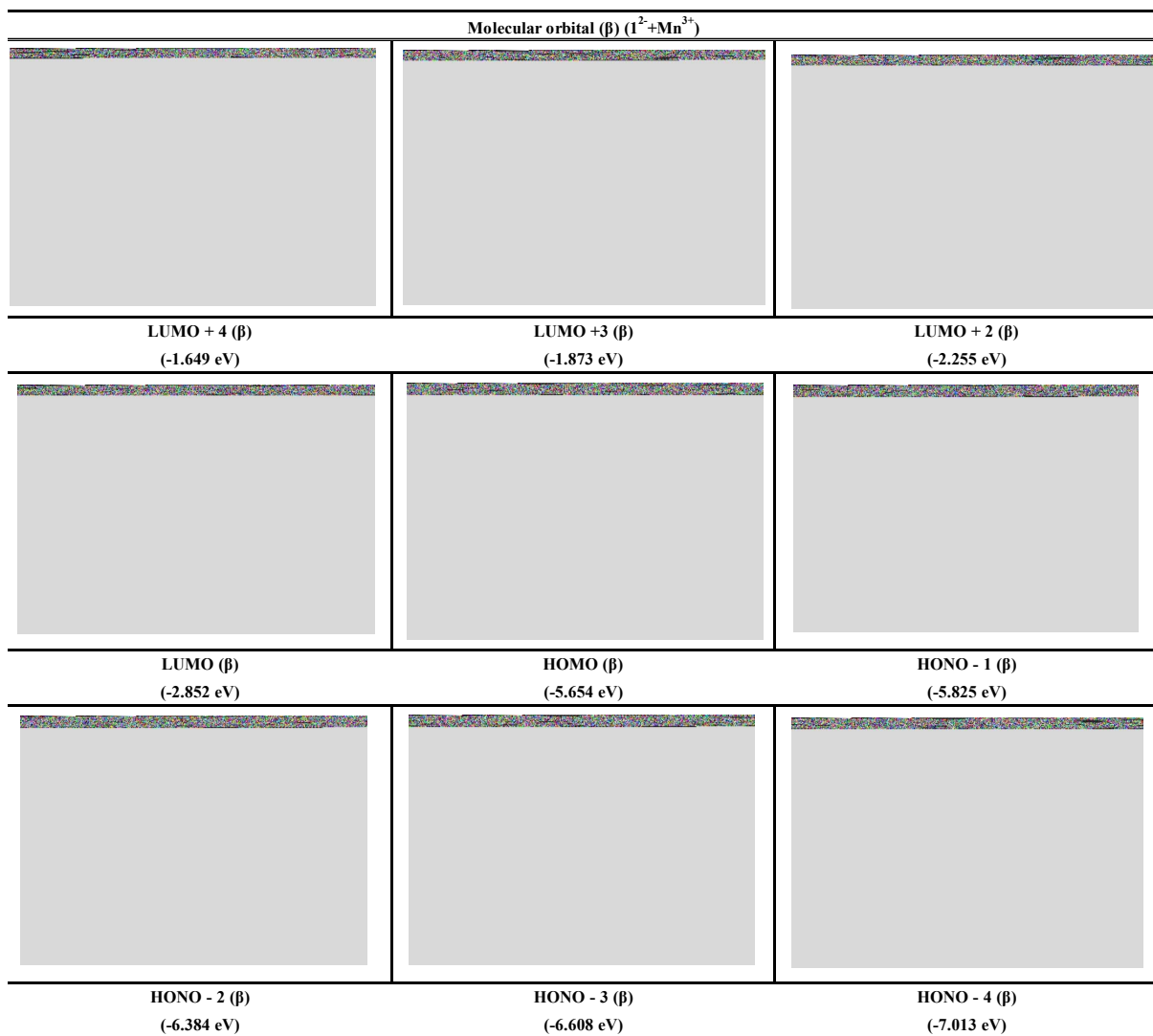


**Fig. S13** Isosurface (0.030 electron bohr<sup>-3</sup>) of molecular orbitals ( $\beta$  spin) participating in the major singlet excited states of **1**-Mn<sup>3+</sup> complex.